

MIT Open Access Articles

Voltage-controlled reversible modulation of colloidal quantum dot thin film photoluminescence

The MIT Faculty has made this article openly available. **Please share** how this access benefits you. Your story matters.

Citation: Xie, Sihan, Zhu, Han, Li, Melissa and Bulović, Vladimir. 2022. "Voltage-controlled reversible modulation of colloidal quantum dot thin film photoluminescence." Applied Physics Letters, 120 (21).

As Published: 10.1063/5.0093248

Publisher: AIP Publishing

Persistent URL: <https://hdl.handle.net/1721.1/145493>

Version: Final published version: final published article, as it appeared in a journal, conference proceedings, or other formally published context

Terms of use: Creative Commons Attribution 4.0 International license



Voltage-controlled reversible modulation of colloidal quantum dot thin film photoluminescence ^{EP}

Cite as: Appl. Phys. Lett. **120**, 211104 (2022); <https://doi.org/10.1063/5.0093248>

Submitted: 27 March 2022 • Accepted: 10 May 2022 • Published Online: 23 May 2022

Published open access through an agreement with Massachusetts Institute of Technology

 Sihan Xie, Han Zhu,  Melissa Li, et al.

COLLECTIONS

 This paper was selected as an Editor's Pick



View Online



Export Citation



CrossMark

ARTICLES YOU MAY BE INTERESTED IN

[Composition gradient-enabled circular photogalvanic effect in inorganic halide perovskites](#)
Applied Physics Letters **120**, 211901 (2022); <https://doi.org/10.1063/5.0083187>

[Direct bandgap GeSn nanowires enabled with ultrahigh tension from harnessing intrinsic compressive strain](#)

Applied Physics Letters **120**, 202103 (2022); <https://doi.org/10.1063/5.0087477>

[Milliwatt-power far-UVC AlGaIn LEDs on sapphire substrates](#)


Applied Physics Letters **120**, 211105 (2022); <https://doi.org/10.1063/5.0088454>

1.8 GHz

8.5 GHz

Trailblazers. New

Meet the Lock-in Amplifiers that measure microwaves.

 Zurich Instruments [Find out more](#)

Voltage-controlled reversible modulation of colloidal quantum dot thin film photoluminescence

Cite as: Appl. Phys. Lett. **120**, 211104 (2022); doi: [10.1063/5.0093248](https://doi.org/10.1063/5.0093248)

Submitted: 27 March 2022 · Accepted: 10 May 2022 ·

Published Online: 23 May 2022



View Online



Export Citation



CrossMark

Sihan Xie,  Han Zhu, Melissa Li,  and Vladimir Bulović^{a)} 

AFFILIATIONS

Research Laboratory of Electronics, Massachusetts Institute of Technology, Cambridge, Massachusetts 02139, USA

^{a)} Author to whom correspondence should be addressed: bulovic@mit.edu

ABSTRACT

Active modulation of quantum dot thin film photoluminescence (PL) has been far-reaching potential applications in biomedical and optoelectronic systems, but challenges remain in achieving large PL modulation depth and fast temporal response. Here, we report an efficient voltage-controlled optical down-converter by optically exciting a colloidal quantum dot thin film within a quantum dot light-emitting diode under reverse bias. Utilizing field-induced luminescence quenching, we show that a large electric field can strongly modify carrier dynamics in this nanostructured device, resulting in stable and reversible photoluminescence quenching. The device exhibits photoluminescence reduction of up to 99.5%, corresponding to a contrast ratio of 200:1 under the applied electric field of 3 MV cm^{-1} with a 300 ns response time. Using excitation wavelength dependent and transient PL spectroscopy, we further show that the high degree of quenching is achieved by a synergistic interplay of quantum-confined Stark effect and field-induced exciton dissociation.

© 2022 Author(s). All article content, except where otherwise noted, is licensed under a Creative Commons Attribution (CC BY) license (<http://creativecommons.org/licenses/by/4.0/>). <https://doi.org/10.1063/5.0093248>

Colloidal quantum dots (QDs) are a class of luminophores that enable applications ranging from biomedical sensing to next generation display and lighting technologies.^{1–4} Substantial progress has been made in the development of solid-state QD light-emitting devices over the years.^{5–10} One central problem that limits the device efficiency is QD photoluminescence (PL) quenching due to either charge accumulation at or near the QD sites^{11,12} or the increased electric field across the QD layer.^{13,14} An external electric field can polarize a QD exciton by physically separating the electron–hole pair in opposite directions.¹⁵ The reduction in wavefunction overlap lowers the radiative recombination rate, quenches QD PL, and is accompanied by a concomitant redshift of the PL spectrum, known as the quantum-confined Stark effect (QCSE).¹⁶ At large electric fields, the coulombic binding of excitons can be overcome, resulting in dissociation and formation of free carriers.¹⁷

Instead of modulating light emission by forming excitons through electrical charge injection, we can leverage the electric-field-induced QD PL quenching processes to control the PL efficiency of an optically excited QD film. Prior to our work, active modulation of the QD PL in a solid state has been demonstrated in a variety of structures, yet the overarching goals of achieving large PL quenching and a fast

temporal response remained an active area of research. Bozyigit *et al.* used a QD capacitor structure to show that the electric field can strongly quench luminance of the QD film in the absence of mobile charge¹⁸ with 90% max PL suppression achieved at an electric field of 4 MV cm^{-1} . Few groups have leveraged QD PL quenching in biological¹⁹ or display²⁰ applications. For instance, Rowland *et al.*, adopting the capacitor structure, utilized QD emission to track the action potential profile of a firing neuron.¹⁹ More recently, Salihoglu *et al.* demonstrated a color-variable PL display that used QD PL quenching to dim selective pixels by directly injecting electric charges into QDs via a graphene layer.²⁰ The ultimate degree of PL quenching achieved in previous studies is summarized in Table S1. Regardless of the cause for the quenching limit, the maximum PL reduction achieved has been 90% (corresponding to the contrast ratio of 10:1) with response time in milliseconds at best.

The observed challenges of limited quenching and slow PL response are both likely associated with screening of the applied electric field by photogenerated, field-ionized, or electrically injected charges. These charges can reside in delocalized band edge states, defect states on the nanocrystal, or electronic states in the surrounding matrix. The application of the electric field is often also associated with

QD charging, even if charging is not the intended outcome. At zero field, a number of studies on single QD blinking^{21,22} show that a photogenerated carrier can be spontaneously ejected to a localized state residing on the QD surface or the surrounding matrix. On an ensemble level, the photogenerated charge can contribute to the screening of the externally applied field,^{23,24} which limits the ultimate degree of achievable field-induced quenching.

In this work, we use a quantum dot light-emitting diode (QD-LED) structure that operates efficiently in forward bias, hence optimized for minimum deleterious charge buildup next to the luminescent QD layer. The device is reverse biased to minimize charge injection from the electrodes into the device. When optically excited to generate the QD PL, the photogenerated charge is rapidly dissociated in the reverse-bias electric field, leading to efficient reduction of the QD PL. Through steady-state and transient PL measurements, we observe up to 99.5% QD PL suppression at 3.3 MV cm^{-1} , corresponding to a contrast ratio of 200:1. The device also demonstrates reversible modulation with a response time of 300 ns and no significant degradation when continuously operated under millisecond pulsed bias. This is the best performance reported to date for an electrically controlled PL device based on colloidal nanocrystals. Using excitation wavelength dependent and time-resolved PL analysis, we find that the high degree of quenching is achieved by QCSE, which is followed by QD exciton dissociation under the reverse-bias electric field.

Our device is comprised of a 10 nm (~ 1 monolayer) thick layer of CdSe/ZnCdS core-shell QDs sandwiched between a ZnO electron transport layer (ETL) and a hole transport layer (HTL) of tris(4-carbazoyl-9-ylphenyl)amine (TCTA). A thin film of aluminum (Al) with molybdenum oxide (MoO_3) underlayer and a film of indium tin oxide (ITO) are used as anode and cathode layers, respectively. The multilayer device is visualized in the cross-sectional scanning electron microscope image, shown in Fig. 1(a), which shows the thickness of each layer. As shown in Fig. S1, the synthesized CdSe/ZnCdS QDs exhibit an emission peaked at $\lambda = 625 \text{ nm}$ with a full width half maximum (FWHM) of 30 nm. The photoluminescence quantum yield (PLQY) of the QD solution and the thin film are measured to be 85% and 75%, respectively. The electroluminescence (EL) performance under forward bias of the QD-LED is also shown in Fig. S2. The device exhibits EL emission peaked at $\lambda = 635 \text{ nm}$ with a peak external quantum efficiency (EQE) of 15.9% at a driving voltage of 2.9 V. Assuming

a light outcoupling efficiency of between 20% and 25%,⁴ the internal quantum efficiency (IQE) of the device is between 65% and 80%, nearly matching the PLQY, and therefore, in a forward-biased device, the QD film is minimally quenched by the surrounding charge transport layers. The energy band diagram of the device is shown in Fig. 1(b).

To study the effect of the applied electric field on the QD PL in this structure, we first perform steady-state measurements by applying reverse bias to the device that is optically excited by $\lambda = 405 \text{ nm}$ light and record the QD PL intensity and spectrum. In the reverse-biased QD-LED, the electric field is dropped across the QD layer but without external charge injection from the device electrodes. As no charge is injected into the device, any observed quenching is related to the applied electric field. We apply 2 ms duration square voltage pulses at 100 Hz repetition rate with amplitudes from 0 up to -20 V , corresponding to electric fields of 0 – 3.3 MV cm^{-1} . The square waveform is selected to minimize the potential permanent electric field induced damage on the QD film. Electric field strength in the QD film is estimated by dividing the applied reverse bias by the total thickness of the QD and HTL films, which have similar dielectric constants.²⁵ The voltage drop across the ZnO film is assumed to be minimal due to its high electron mobility.^{26–28} We note that the internal field inside the QD is lower due to dielectric screening from QD surfaces.^{16,25} The precise value of the internal field is difficult to calculate due to the anisotropic, heterogeneous, and partially disordered local environment. As shown in Fig. 2(a), the steady-state QD PL spectra are plotted with increasing electric field strength. The PL intensity is fully recovered after the electric field is removed, as shown by the good match in Fig. 2(a) between the solid and dashed spectra that are both obtained at 0 V applied bias. In addition to the PL intensity decrease, the PL spectra also display a redshift, as expected from QCSE of CdSe QDs. The integrated PL intensity (normalized to the intensity at zero bias) is shown in Fig. 2(b). The device exhibits a maximum 99.5% PL quenching under at 3.3 MV cm^{-1} , corresponding to a contrast ratio of 200:1. No further improvement of PL quenching is observed beyond -20 V . The CCD camera image of the QD-LED pixel under the microscope starts to show residual emission from isolated spots at -24 V , as illustrated in Fig. S3, which is suggestive of the dielectric breakdown at the very high reverse bias.^{29,30} To confirm that the increasing reverse bias leads to an increasing electric field and no charge injection, we measure the device current under reverse bias up to -20 V and show that the leakage current is only on the order of few μA , as shown in Fig. S5.

To evaluate whether the applied electric field is screened by charges, we apply an extended bias pulse to monitor the temporal evolution of the QD PL. Figure 3(a) displays the PL time traces of the device under 5 s square voltage pulses from 0 to -20 V . By overlaying the different traces, we can compare both the maximum PL reduction and the quenching dynamics. In addition to the expected nearly instantaneous PL intensity reduction at the beginning of the electric field application, we also observe a slow recovery in the PL intensity while the bias is held constant. We note this PL transient dynamics is more prominent at the lower field (0.7 MV cm^{-1}) but is almost completely suppressed at -20 V . The fact that these dynamics occur on a time scale of hundreds of milliseconds to seconds are consistent with charge buildup in our devices at lower fields. Since we do not have significant charge injection under reverse bias operation, this

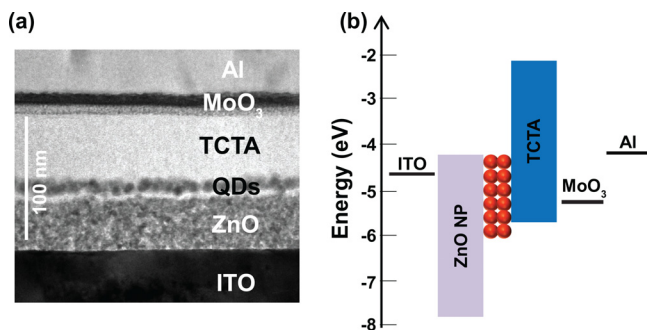


FIG. 1. (a) Cross-sectional SEM image of the QD-LED prepared by focused ion beam showing each layer of the device. (b) Flat band energy diagram of constituent layers on an energy scale referenced to the vacuum level.

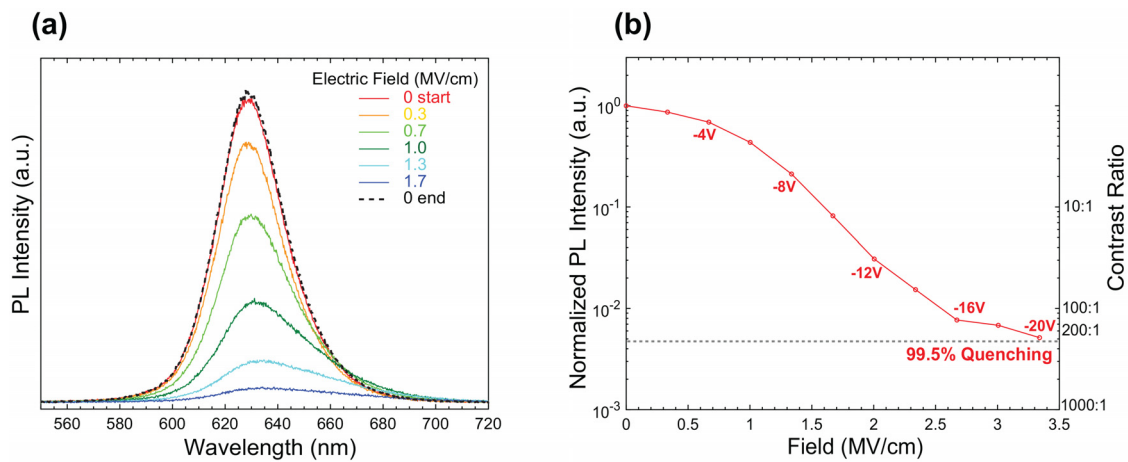


FIG. 2. (a) Steady state PL spectra of a QD-LED with a 10 nm thick QD film, optically excited with $\lambda = 405$ nm light. Drop in the PL intensity and a redshift in the peak PL wavelength is observed with increasing reverse-biased electric field. (b) Integrated PL intensity (normalized) as a function of the applied electric field shows the maximum achievable quenching of 99.5% at 3.3 MV cm^{-1} .

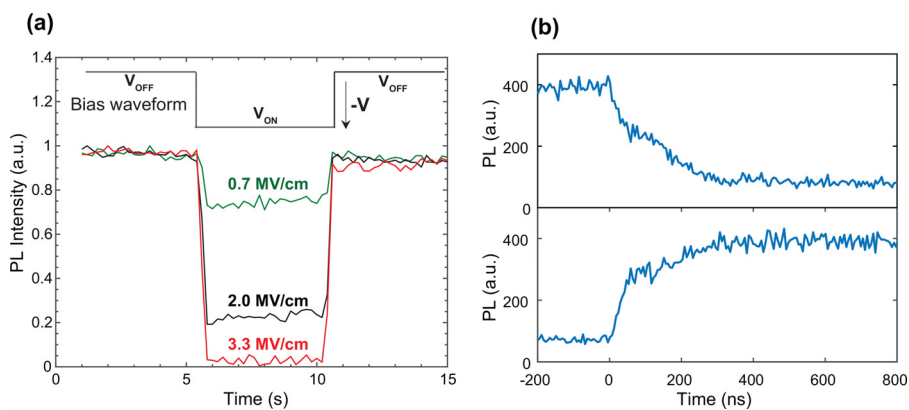


FIG. 3. (a) Time traces of the device as a function of the applied electric field showing the reversible modulation of the PL intensity. Inset: Applied bias waveform. (b) PL intensity measured at the start (top) and the end (bottom) of a -10 V pulse for a device with a 10 nm thick QD layer.

could be a result of ionization of photogenerated charges. Either the extracted charge or the opposite charge that is left on the QD screens the external electric field, thereby reduces the amount of field-induced quenching on the nearby QDs. In addition to the constant-bias dynamics, the time response of the device at the start and end of the voltage pulse is measured using an avalanche photodiode (APD), as shown in Fig. 3(b). The device exhibits a fast response time of about 100 and 300 ns to reach 50% and 90% of the maximum quenching, respectively.

In order to identify the mechanisms behind field-induced PL quenching, we investigate exciton decay dynamics at different applied electric fields using time-resolved photoluminescence (TRPL) measurements. Figure 4 shows QD PL time transients under increasing electric fields from 0 to 1.7 MV cm^{-1} . It is noted that the TRPL measurement is limited by insufficient PL signals beyond -10 V (1.7 MV cm^{-1}) due to efficient PL quenching. The normalized traces (in the inset) show that the PL decay becomes faster with increasing field. All decay curves are fitted to a bi-exponential function. The resulting decay lifetimes are extracted and shown in Table I. Two decay lifetimes, τ_1 and τ_2 , exhibit distinct trends as the electric field is

increased from 0 to 1.7 MV cm^{-1} . While τ_1 shows a marked decrease from 8.6 to 3.0 ns, τ_2 displays a small change in the range of 20–23 ns. This trend differs from multiple earlier investigations, in which the PL decay lifetimes remained constant with the electric field.^{13,18,19} We note that the higher luminescence efficiency of QDs used in this work would make our QD luminescence lifetimes particularly susceptible to the introduction of a nonradiative pathway such as the field-induced exciton dissociation. Also, the primary difference between our device and those in the earlier reports is the existence of the charge transport interfaces sandwiching the 1–2 monolayers of the QD film, facilitating rapid transport of photogenerated charges away from the QD.

The QD film in the reverse-biased QD-LED can act as a photoactive layer, where upon optical excitation of a QD, the excited carrier can be swept out of the QD into the neighboring charge transport layer. This charge extraction process is easier for hot carriers, which are generated by photons whose energy is significantly larger than the QD core bandgap energy. Mashford *et al.* have previously demonstrated, by using kelvin probe measurements of QD films on top of ZnO nanoparticle films, that photoelectrons are extracted from CdSe/CdS core-shell QDs and transferred to ZnO when excited by high

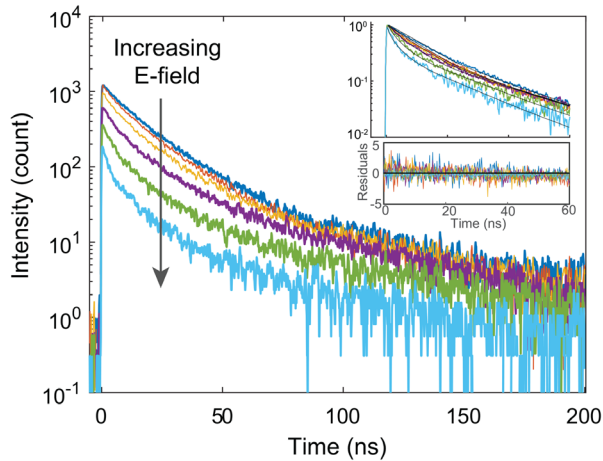


FIG. 4. Time-resolved PL decays of a QD-LED with 10 nm thick QD layer reverse biased with increasing electric fields from 0 to 1.7 MV cm^{-1} . The device is excited using a $\lambda = 405 \text{ nm}$ pulsed laser. Inset: normalized decay traces with bi-exponential fit function (black solid line) and bottom panel displaying residuals of the fit.

optical excitation energy (above the QD bandgap).³¹ Other reports have shown that the relative rate of charge extraction vs relaxation to the band edge is dependent on the excitation energy in QDs,^{32,33} and this can lead to an excitation energy dependence of the PL if the trapped charges are ultimately extracted by the electrodes or if they recombine through nonradiative channels.^{34,35} To investigate this carrier extraction process, we measure the steady-state PL quenching of the QD film that is excited with different excitation wavelengths, swept from $\lambda = 460$ to $\lambda = 560 \text{ nm}$, as shown in Fig. 5. No significant change in the amount of PL quenching for different excitation wavelengths is observed until the applied bias reaches -8 V (1.3 MV cm^{-1}). As we keep increasing the electric field, the device shows a sharper drop in PL with higher photon energy excitations. At -20 V , bias quenching of QD PL generated by $\lambda = 460 \text{ nm}$ excitation is a factor of 3.5 more efficient than the quenching of the QD PL generated by $\lambda = 560 \text{ nm}$ excitation. The dependence of the PL quenching efficiency on the energy of the excitation light is consistent with field-induced extraction of photogenerated charges out of the QDs, a process which is more efficient when hot carriers are generated. Given the amorphous structure of QD interfaces with neighboring charge transport layers, it is likely that the energy barrier for charge extraction is different locally

TABLE I. Decay lifetimes as a function of the applied electric field.

E-field (MV cm^{-1})	τ_1 (ns)	τ_2 (ns)	A_1	A_2	Relative fraction	
0	8.6	22.6	618	647	0.489	0.511
0.3	6.1	20.1	518	720	0.419	0.581
0.7	5.6	21.2	489	502	0.493	0.507
1	5.1	22.6	375	267	0.584	0.416
1.3	5.0	23.1	242	125	0.659	0.341
1.7	3.0	20.5	124	63	0.664	0.336

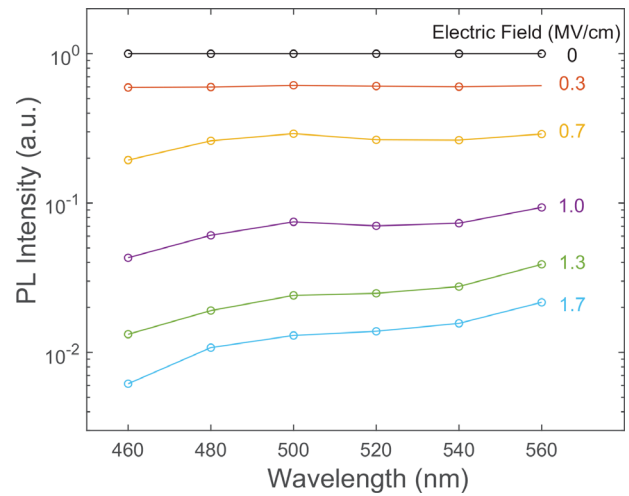


FIG. 5. Integrated PL intensity (normalized) of the device as a function of the excitation wavelength (from $\lambda = 460$ to $\lambda = 560 \text{ nm}$) with increasing applied electric field.

for different individual QDs. As a result, even at higher electric fields, charge extraction from some of the individual QDs could be impeded. This subset of QDs (which we will refer to as QD subset 2) would have an average PL lifetime τ_2 of 21.7 ns for different bias conditions, just as observed in our time-resolved fits of the QD PL at different biases (Table I). Our measured τ_2 lifetime is also consistent with previous observations, which have shown 20–30 ns radiative lifetime of neutral excitons in PL-efficient CdSe QDs.^{22,36} The other subset of QDs (which we will refer to as QD subset 1) manifests a reduced effective PL lifetime, τ_1 in Table I, as the field-induced charge extraction process dissociates the excitons on these QDs, introducing a nonradiative process that is more-rapid than the radiative recombination. The fractional areas under the decay curve, A_1 and A_2 , that have lifetimes τ_1 and τ_2 , respectively, represent the relative contributions to the measured QD PL from the two subsets of luminescing QDs. Both A_1 and A_2 drop with the increasing electric field, with A_2 decreasing more rapidly.

These two subsets of QDs are also evident in the PL spectra taken at different electric fields, shown in Fig. 2(a). The measured PL spectra can be fitted by using two Voigt functions, as shown in Fig. S4(a) for QD PL spectra at fields of 0 and 1.7 MV cm^{-1} . Figure S4(b) plots the peak wavelength of the two Voigts, labeled as peak 1 (low energy, high wavelength peak) and peak 2 (high energy, low wavelength peak) for different electric fields. With increasing electric field, it is evident that peak 1 is strongly red-shifted (from $\lambda = 635$ to $\lambda = 653 \text{ nm}$), while peak 2 is relatively steady with the redshift of only 2 nm. Given that the PL peak wavelength of our QDs in a solution is $\lambda = 625 \text{ nm}$, we associate peak 2 with the QD subset 2, whose TRPL decay lifetime is τ_2 . In addition, the relative fraction of peak 2 drops from 53% at 0 MV cm^{-1} to 25% at 1.7 MV cm^{-1} , shown in Fig. S4(c), which is consistent with the TRPL lifetime results for QD subset 2 in Table I. The redshift of peak 1 is consistent with the QCSE and is there accompanied by the reduction in radiative rates. This makes the QDs relatively less competitive with nonradiative processes, resulting in more rapid PL dynamics, just as we see for QD subset 1 in our TRPL traces.

In summary, we demonstrate that QD-LEDs can be used as efficient voltage-controlled optical down-converters when operating under reverse bias. We use field-induced QD luminescence quenching in our favor and show efficient PL modulation of up to 99.5% (200:1 contrast ratio) under 3 MV cm^{-1} with 300 ns response time, giving us the best performing electrically controlled QD PL device to date. Using optical spectroscopy, we further show that a large electric field can strongly modify carrier dynamics in a nanostructure, and the stable and repeatable quenching is accomplished by QCSE and field-induced exciton dissociation. Quantifying the time-resolved spectroscopic data, as well as the observed spectral shifts due to the quantum-confined Stark effect, we are able to numerically match the observed PL quenching, providing a comprehensive physical mechanism for the observations. The results presented here open up additional research directions as similar device structures could be used in electro-optic modulators or electrically tuned PL display technology.

See the [supplementary material](#) for the absorption and PL spectra of the quantum dots in a solution, device performance under forward bias, CCD camera images of the device under a microscope, PL spectrum fitting, and current–voltage characteristics of the device under reverse bias.

The project was initiated under the Center for Excitonics, an Energy Frontier Research Center funded by the U.S. Department of Energy, Office of Science, and Office of Basic Energy Sciences under Award No. DE-SC0001088 (MIT). The project was completed with support of the Material and Device Research Institute of the Samsung Advanced Institute of Technology (SAIT). The authors thank Robert Nick for kindly providing the colloidal quantum dot solution and thank Michel Nasilowski for providing the ZnO nanoparticle solution.

AUTHOR DECLARATIONS

Conflict of Interest

The authors have no conflicts to disclose.

Author Contributions

S.H.X. and H.Z. contributed equally to this work.

DATA AVAILABILITY

The data that support the findings of this study are available from the corresponding author upon reasonable request.

REFERENCES

- ¹Y. Shirasaki, G. J. Supran, M. G. Bawendi, and V. Bulović, *Nat. Photonics* **7**, 13 (2013).
- ²G. J. Supran, Y. Shirasaki, K. W. Song, J.-M. Caruge, P. T. Kazlas, S. Coe-Sullivan, T. L. Andrew, M. G. Bawendi, and V. Bulović, *MRS Bull.* **38**, 703 (2013).
- ³J. M. Pietryga, Y.-S. Park, J. Lim, A. F. Fidler, W. K. Bae, S. Brovelli, and V. I. Klimov, *Chem. Rev.* **116**, 10513 (2016).
- ⁴X. Dai, Y. Deng, X. Peng, and Y. Jin, *Adv. Mater.* **29**, 1607022 (2017).
- ⁵W. Cao, C. Xiang, Y. Yang, Q. Chen, L. Chen, X. Yan, and L. Qian, *Nat. Commun.* **9**, 2608 (2018).
- ⁶H. Shen, Q. Gao, Y. Zhang, Y. Lin, Q. Lin, Z. Li, L. Chen, Z. Zeng, X. Li, Y. Jia, S. Wang, Z. Du, L. S. Li, and Z. Zhang, *Nat. Photonics* **13**, 192 (2019).
- ⁷Y.-H. Won, O. Cho, T. T. Kim, D.-Y. Chung, T. Kim, H. Chung, H. Jang, J. Lee, D. Kim, and E. Jang, *Nature* **575**, 634 (2019).
- ⁸J. H. Chang, P. Park, H. Jung, B. G. Jeong, D. Hahm, G. Nagamine, J. Ko, J. Cho, L. A. Padilha, D. C. Lee, C. Lee, K. Char, and W. K. Bae, *ACS Nano* **12**, 10231 (2018).
- ⁹T. Davidson-Hall and H. Aziz, *Appl. Phys. Lett.* **116**, 010502 (2020).
- ¹⁰T.-H. Kim, K.-S. Cho, E. K. Lee, S. J. Lee, J. Chae, J. W. Kim, D. H. Kim, J.-Y. Kwon, G. Amaratunga, S. Y. Lee, B. L. Choi, Y. Kuk, J. M. Kim, and K. Kim, *Nat. Photonics* **5**, 176 (2011).
- ¹¹J. F. Wager and P. D. Keir, *Annu. Rev. Mater. Sci.* **27**, 223 (1997).
- ¹²V. I. Klimov, *Science* **287**, 1011 (2000).
- ¹³Y. Shirasaki, G. J. Supran, W. A. Tisdale, and V. Bulović, *Phys. Rev. Lett.* **110**, 217403 (2013).
- ¹⁴D. Bozyigit and V. Wood, *MRS Bull.* **38**, 731 (2013).
- ¹⁵S.-J. Park, S. Link, W. L. Miller, A. Gesquiere, and P. F. Barbara, *Chem. Phys.* **341**, 169 (2007).
- ¹⁶S. A. Empedocles and M. G. Bawendi, *Science* **278**, 2114 (1997).
- ¹⁷R. Scott, A. W. Achtstein, A. V. Prudnikau, A. Antanovich, L. D. A. Siebbeles, M. Artemyev, and U. Woggon, *Nano Lett.* **16**, 6576 (2016).
- ¹⁸D. Bozyigit, O. Yarema, and V. Wood, *Adv. Funct. Mater.* **23**, 3024 (2013).
- ¹⁹C. E. Rowland, K. Susumu, M. H. Stewart, E. Oh, A. J. Mäkinen, T. J. O’Shaughnessy, G. Kushto, M. A. Wolak, J. S. Erickson, A. L. Efros, A. L. Huston, and J. B. Delehanty, *Nano Lett.* **15**, 6848 (2015).
- ²⁰O. Salihoglu, N. Kakenov, O. Balci, S. Balci, and C. Kocabas, *ACS Photonics* **5**, 2384 (2018).
- ²¹A. L. Efros and D. J. Nesbitt, *Nat. Nanotechnol.* **11**, 661 (2016).
- ²²C. Galland, Y. Ghosh, A. Steinbrück, M. Sykora, J. A. Hollingsworth, V. I. Klimov, and H. Htoon, *Nature* **479**, 203 (2011).
- ²³M. Moebius, J. Martin, M. Hartwig, R. R. Baumann, T. Otto, and T. Gessner, *AIP Adv.* **6**, 085309 (2016).
- ²⁴R. Korlacki, R. F. Saraf, and S. Ducharme, *Appl. Phys. Lett.* **99**, 153112 (2011).
- ²⁵D. Bozyigit, V. Wood, Y. Shirasaki, and V. Bulovic, *J. Appl. Phys.* **111**, 113701 (2012).
- ²⁶H.-I. Baek and C. Lee, *J. Appl. Phys.* **103**, 54510 (2008).
- ²⁷J. Kwak, W. K. Bae, D. Lee, I. Park, J. Lim, M. Park, H. Cho, H. Woo, D. Y. Yoon, K. Char, S. Lee, and C. Lee, *Nano Lett.* **12**, 2362 (2012).
- ²⁸N. Kirkwood, B. Singh, and P. Mulvaney, *Adv. Mater. Interfaces* **3**, 1600868 (2016).
- ²⁹T. B. Tran, I. S. Beloborodov, X. M. Lin, T. P. Bigioni, V. M. Vinokur, and H. M. Jaeger, *Phys. Rev. Lett.* **95**, 076806 (2005).
- ³⁰V. Wood, M. J. Panzer, D. Bozyigit, Y. Shirasaki, I. Rousseau, S. Geyer, M. G. Bawendi, and V. Bulović, *Nano Lett.* **11**, 2927 (2011).
- ³¹B. S. Mashford, M. Stevenson, Z. Popovic, C. Hamilton, Z. Zhou, C. Breen, J. Steckel, V. Bulovic, M. Bawendi, S. Coe-Sullivan, and P. T. Kazlas, *Nat. Photonics* **7**, 407 (2013).
- ³²W. A. Tisdale, K. J. Williams, B. A. Timp, D. J. Norris, E. S. Aydil, and X.-Y. Zhu, *Science* **328**, 1543 (2010).
- ³³J. A. McGuire, M. Sykora, I. Robel, L. A. Padilha, J. Joo, J. M. Pietryga, and V. I. Klimov, *ACS Nano* **4**, 6087 (2010).
- ³⁴D. Roy, A. Das, C. K. De, S. Mandal, P. R. Bangal, and P. K. Mandal, *J. Phys. Chem. C* **123**, 6922 (2019).
- ³⁵M. Righetto, A. Minotto, and R. Bozio, *J. Phys. Chem. C* **121**, 896 (2017).
- ³⁶J. Lim, B. G. Jeong, M. Park, J. K. Kim, J. M. Pietryga, Y.-S. Park, V. I. Klimov, C. Lee, D. C. Lee, and W. K. Bae, *Adv. Mater.* **26**, 8034 (2014).